Finite Element Investigations on the Interaction between a Pile and Swelling Clay

Kaufmann, Kristine Lee; Nielsen, Benjaminn Nordahl; Augustesen, Anders Hust

Publication date:
2010

Document Version
Publisher's PDF, also known as Version of record

Finite Element Investigations on the Interaction between a Pile and Swelling Clay

K. L. Kaufmann
B. N. Nielsen
A. H. Augustesen

ISSN 1901-726X
DCE Technical Report No. 104

AALBORG UNIVERSITY
Department of Civil Engineering

Aalborg University
Department of Civil Engineering
Water & Soil

DCE Technical Report No. 104

Finite Element Investigations on the Interaction between a Pile and Swelling Clay

by

K. L. Kaufmann
B. N. Nielsen
A. H. Augustesen

September 2010

Scientific Publications at the Department of Civil Engineering

Technical Reports are published for timely dissemination of research results and scientific work carried out at the Department of Civil Engineering (DCE) at Aalborg University. This medium allows publication of more detailed explanations and results than typically allowed in scientific journals.

Technical Memoranda are produced to enable the preliminary dissemination of scientific work by the personnel of the DCE where such release is deemed to be appropriate. Documents of this kind may be incomplete or temporary versions of papers—or part of continuing work. This should be kept in mind when references are given to publications of this kind.

Contract Reports are produced to report scientific work carried out under contract. Publications of this kind contain confidential matter and are reserved for the sponsors and the DCE. Therefore, Contract Reports are generally not available for public circulation.

Lecture Notes contain material produced by the lecturers at the DCE for educational purposes. This may be scientific notes, lecture books, example problems or manuals for laboratory work, or computer programs developed at the DCE.

Theses are monograms or collections of papers published to report the scientific work carried out at the DCE to obtain a degree as either PhD or Doctor of Technology. The thesis is publicly available after the defence of the degree.

Latest News is published to enable rapid communication of information about scientific work carried out at the DCE. This includes the status of research projects, developments in the laboratories, information about collaborative work and recent research results.

Published 2010 by
Aalborg University
Department of Civil Engineering
Sohngaardsholmsvej 57,
DK-9000 Aalborg, Denmark

Printed in Aalborg at Aalborg University

ISSN 1901-726X
DCE Technical Report No. 104

Finite Element Investigations on the Interaction between a Pile and Swelling Clay

K. L. Kaufmann[1], B. N. Nielsen[2] and A. H. Augustesen[3]

Aalborg University, September 2010

Abstract

This paper aims to investigate the interaction between a pile and a swelling soil modelled as a cohesive soil subjected to unloading. The investigations include analyses of the heave of the excavation level, shear stresses at the soil–pile interface and internal pile forces based on a case study of Little Belt Clay. The case study involves a circular concrete pile installed in clay immediately after an excavation. The influence of the swelling soil on the soil–pile interaction and the internal pile forces are analysed by solely observing the upper pile part positioned in the swelling zone. For the investigated case study, the influence of the pile is observed in a radius of approximately 3 pile diameters from the pile centre creating a weak zone inside this radius. The maximum heave of the excavation level inside this radius decreases polynomially with increasing interface strength. The swelling of the surrounding soil implies upward shear stresses at the soil–pile interface leading to tensile vertical stresses in the pile. In the current case, they exceed the tensile strength of concrete. The tensile vertical stresses peak after 35-50 years. However, the heave of the soil continues for additional 300 years. It appears that the development of plastic interface implies the shrinkage of the pile.

Keywords: Swelling soil, single pile, soil–pile interaction, finite element modelling.

1 Introduction

When clay with a moderate to high activity is exposed to changes in moisture content, the increase in volume known as swelling occurs. The changes in moisture content may appear as an effect of unloading, e.g. an excavation, leading to an undrained response of soil.

Immediately after an unloading, a decrease in the pore pressures is observed. When drainage begins, the pore pressures increase resulting in decreasing effective stresses and, thus, increasing volume of voids, i.e. swelling. The stress variation during an unloading situation can be seen in Fig. 1. The depth to which swelling occurs is named the swelling zone.

[1]Graduate Student, Dept. of Civ. Eng., Aalborg University, Denmark.

[2]Assistant Professor, M.Sc., Dept. of Civ. Eng., Aalborg University, Denmark.

[3]Specialist in Geotechnical Engineering, Ph.D., M.Sc., COWI A/S. Part-time lecturer, Dept. of Civ. Eng., Aalborg University, Denmark.

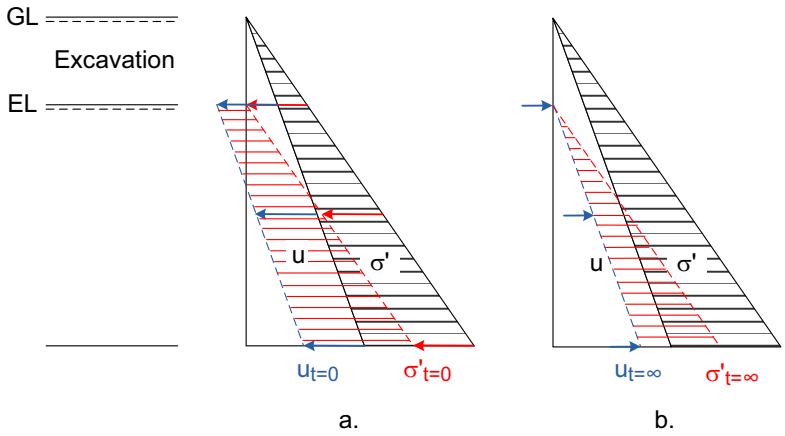

Figure 1: Stress variation for unloading by excavation. a. Total stresses σ, marked by the red dashed line, as a result of pore water pressures u, marked by the blue dashed line, and effective stresses σ', indicated by the hatched red area, immediately after unloading ($t = 0$). b. σ, u and σ' after increase of pore water pressure to an equilibrium state ($t = \infty$). The arrows show the change of stresses from the prior state to the current. GL is ground level and EL is excavation level.

Pile foundation is a common method of reducing settlements when buildings are situated on settlement-inducing soil layers. Due to the skin friction of the pile, the settlements imply downward movement and compressive loading of the pile.

Pile foundations designed to resist compressive loads are occasionally situated in swelling soils. Due to the friction between pile and soil, the heave caused by swelling leads to an additional tensile loading. The mechanisms are simplified in Fig. 3. In Fig. 3a, the pile is driven into the soil and axially loaded implying upward shear stresses at the soil–pile interface. Over time, the swelling implies heave of the ground surface leading to downward shear stresses at the interface inside the swelling zone, cf. Fig. 3b and Fig. 3c. Furthermore, the figures show that the height of the swelling zone n is increasing with time. Fig. 3c is divided into two parts, which can be analysed separately: Fig. 3d and Fig. 3e.

In this paper, focus is paid to the mechanisms of Fig. 3d by numerical analyses. This includes investigations on the heave of the ground surface, the shear stresses at the soil–pile interface and the internal forces in the pile. The analyses are based on a case study of a circular concrete pile installed in the swelling Little Belt Clay.

Initially, the geometrical model is validated by comparison of theoretical approaches and results of a model solely consisting of a swelling soil. Then, a single pile situated in the soil is modelled and the results comprising heave, shear stresses at the interface and internal normal stresses in the pile are analysed.

The positive stress directions used in this paper can be seen in Fig. 2. However, compressive stresses and pore pressures in the soil are defined positive in accordance with common geotechnical practice.

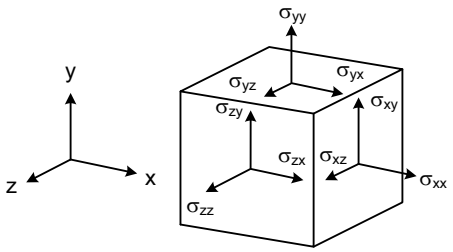

Figure 2: Coordinate system and sign convention of stresses.

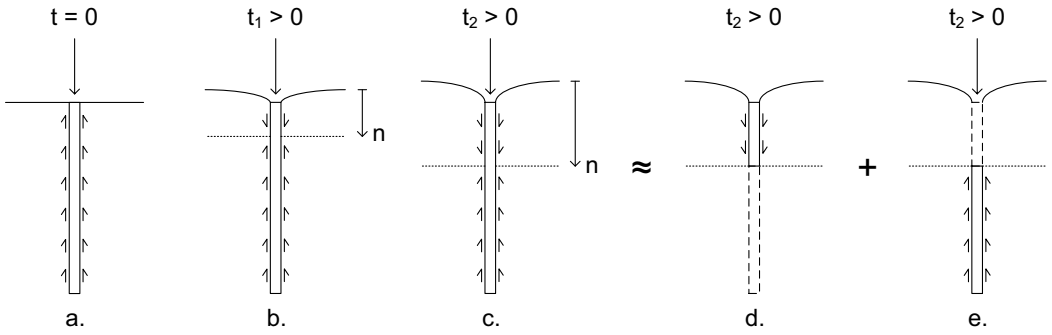

Figure 3: Simplification of the mechanisms for an axially loaded pile in a swelling soil. n is the height of the swelling zone. $t_1 < t_2$.

2 Review of Existing Literature

Swelling soils and piles situated in these soils have been analysed by several different methods in the existing literature. A review of three analysis methods are presented in the following to gain an insight to the difficulties of analysing swelling soils.

2.1 Okkels and Bødker, 2008

Okkels and Bødker (2008) aim to determine the height of the swelling zone n and the magnitude and time frame of the consequently heave by a simple first order theory. As an approximation, the one-sided drainage is assumed to be linearly distributed, cf. Fig. 4. The approximation is based on an expression of the height of the swelling zone n as a function of time. The approximation has shown to yield satisfactory results.

n is determined by equalising the incoming volume of water and the heave at a specific time calculated as consolidation settlements of preconsolidated clay. The progress of the n with time for a coefficient of consolidation of $c_k = 10^{-8}$ m^2/s can be seen in Fig. 5.

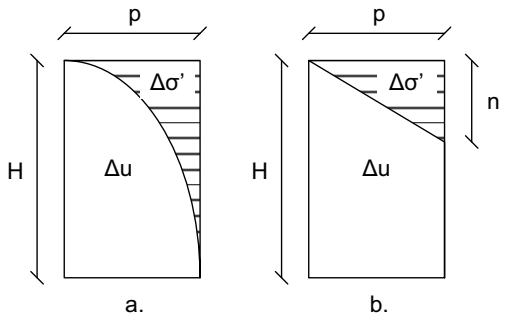

Figure 4: Stress variation for consolidation with one-sided drainage where H is the height of the layer, p the unloading pressure, Δu the excess pore pressure and $\Delta\sigma'$ the effective stress variation. a. One-sided drainage by Terzaghi's theory of consolidation. b. Linear approximation where n is the height of the swelling zone.

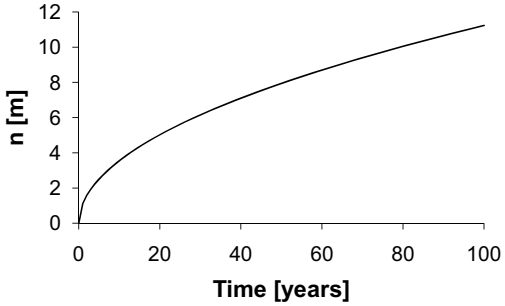

Figure 5: Progress of the height of the swelling zone with time for $c_k = 10^{-8}$ m^2/s.

The pore pressure is determined by the height of the swelling zone by which the total heave is calculated similar to settlements of a thin layer of normally consolidated clay by the conventional theory of consolidation. For this calculation, the compression index for the unloading path

C_{cu} is applied. Whether this index or the compression index for the primary path $C_{c\varepsilon}$ should be applied is debatable.

2.2 Moust Jacobsen and Gwizdala, 1992

The numerical approach in Moust Jacobsen and Gwizdala (1992) describes a method of determining the downward displacement through the pile and of the ground surface caused by settlements. The aim of the approach is to differentiate between the displacement of the pile shaft and the pile toe due to differences in load–displacement curves. The results are then combined to determine the total displacements. Even though the method is developed for loading situation, it is assumed to apply for unloading situations as well. Hereby, the upward displacements of the pile toe and the ground surface caused by heave can be determined.

2.3 Poulos and Davis, 1980

According to Poulos and Davis (1980), the heave of a pile in swelling soil can be determined by a reduction of the displacement at far field, i.e. of the soil without influence of the pile, due to the soil–pile interaction. According to the basic theory proposed by Poulos and Davis (1980), the pile displacements in a swelling soil are determined by elastic calculations.

The basic theory is modified to account for slip in the soil–pile interface, compressive and tensile failure of the pile, layered soil and variation in time. Slip is taken into account by introducing a limited shear stress at the interface τ_i. The limit, i.e. the strength of the interface, is equalised to the Coulomb failure criterion.

2.4 Overview of Existing Literature

An overview of the influencing parameters of the existing theory can be seen in Tab. 1. O&B is an abbreviation of Okkels and Bødker (2008), MJ&G is Moust Jacobsen and Gwizdala (1992) and P&D is Poulos and Davis (1980).

Table 1: Parameters of influence of the existing theory. Index s is for soil and i for interface. L is pile length and D is pile diameter.

O&B	MJ&G	P&D
n	n	n
γ_s	γ_s	Swelling profile
Surface load	Surface load	E_s
c_k	Factor of	ν_s
Time	regeneration	Distribution of τ_i
C_{cu}	Pile diameter	Pile diameter
	Pile material	L/D
	c_u	Axial load on pile
		Tensile failure of pile
		If slip in interface: shear strength

The theory of Okkels and Bødker (2008) is used in the case study to determine the height of the swelling zone n. The remaining two theories of the literature are both based on floating piles. This differ from the concept of Fig. 3d, which is analysed in this paper, where the pile is fixed at the bottom of the model, cf. Sec. 3. Therefore, the latter two theories are not used further.

3 Case Study

The numerical modelling is conducted by the commercial FEM program PLAXIS 2D version 9.02. The case study involves a circular concrete pile with the dimensions $L = 20$ m and $D = 0.34$ m placed in clay immediately after a 10 m excavation of the overlying soil.

The outer width of the soil mass is chosen as $B = 20$ m. This complies with the recommendation by Abbas et al. (2008) of $B = 40D \approx 14$ m. It is assumed that the influence of the swelling soil on the soil–pile interaction and the internal forces in the pile can be analysed by solely observing the upper pile part positioned in the swelling zone. Thus, the height of the model is chosen equal to the height of the swelling zone n determined by Eq. 1 (Okkels and Bødker, 2008).

$$n = 2\sqrt{c_k \cdot t} \tag{1}$$

Where $c_k = \frac{k \cdot E_{oed}}{\gamma_w}$ is the coefficient of consolidation and t is the consolidation time. The soil parameters are listed in Tab. 2 and a life expectancy of $t = 100$ years is chosen. Hereby, the height of the model after the excavation is found to be 11 m.

Because of the circular pile, an axisymmetric model is chosen to study the problem, cf. Fig. 6.

The soil material is applied corresponding to the tertiary swelling clay, Little Belt Clay, and the pile is modelled as concrete. The material parameters of the clay are a combination of a sample with $w = 33.3$ %, $I_P = 183.8$ % and $\sigma'_{pc} = 550$ kPa defined by Thøgersen (2001) and the undrained and effective strength parameters defined by Harremoës et al. (1997). It should be noted, though, that

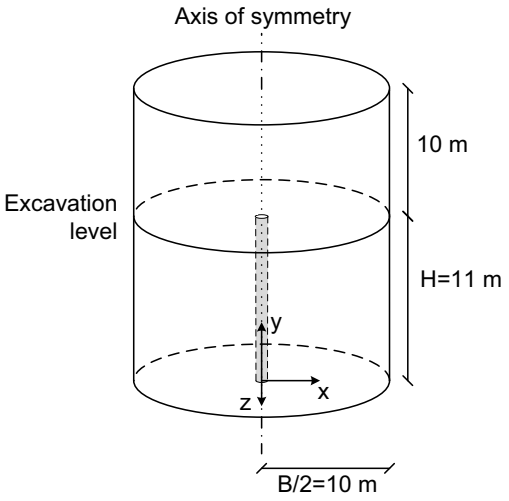

Figure 6: Dimensions of the soil model for the analysed case study. The diameter of the pile is $D = 0.34$ m.

the values of the coeficcients of permeability and the Young's moduli of elasticity are chosen. The moduli are estimated based on the relations $E_{50} = E_{oed}$ and $E_{ur} = 3 \cdot E_{oed}$ (Brinkgreve et al., 2008a). The material parameters for the materials are listed in Tab. 2.

Table 2: Material properties of the case study.

Parameter	Little Belt Clay	Concrete
w [%]	33.3	-
I_P [%]	183.8	-
σ'_{pc} [kPa]	550	-
γ_{sat} [kN/m^3]	18.49	-
γ_{unsat} [kN/m^3]	16.49	24
k_x [m/s]	10^{-11}	-
k_y [m/s]	10^{-11}	-
ν [-]	0.3	0.15
c'/c_u [kPa]	40/225	-
E_{oed} [MPa]	10	$34.8 \cdot 10^3$
E_{50} [MPa]	10	-
E_{ur} [MPa]	30	-
φ' [°]	16	-
ψ [°]	0	-

The soil is modelled as an undrained Hardening Soil (HS) material and the pile as a non-porous linear elastic material. The HS material model is chosen to account for the increase in stiffness appearing for unloading situations by use of the

unloading–reloading modulus E_{ur} and the stress dependency of Young's moduli of elasticity. However, the power for stress–level dependency of stiffness m is chosen equal to zero for simplification. The model parameters for the materials are listed in Tab. 3.

Table 3: Model properties of the case study.

Parameter	Little Belt Clay	Concrete
Model type	Hardening-Soil	Linear elastic
Behaviour	Undrained	Non-porous
K_0 [-]	1	1
OCR [-]	1	-
POP [-]	0	-
R_{inter}	0.267	-
m	0	0

The strength reduction factor R_{inter} is determined as the ratio of the interface cohesion c_i to the undrained shear strength of the soil c_u. The interface cohesion is chosen as $c_i = 60$ kPa in accordance with Danish practice based on the assumption of an undrained failure at the interface, the undrained shear strength c_u and the factors of material and regeneration as $m = 1$ and $r = 0.4$. This leads to the strength reduction factor $R_{inter} = 0.267$. It should be noted that there has not been distinguished between a compressive or a tensile failure at the interface.

If the API Recommended Practice is applied instead of the Danish practice, R_{inter} can be equalised to the dimensionless factor α in Eq. 2 (API, 2000).

$$c_i = \alpha \cdot c_u \tag{2}$$

α is determined by Eqs. 3 and 4.

$$\alpha = 0.5 \cdot \psi^{-0.5} \quad \text{for } \psi \leq 1.0 \tag{3}$$

$$\alpha = 0.5 \cdot \psi^{-0.25} \quad \text{for } \psi > 1.0 \tag{4}$$

Where $\psi = c_u / p'_O$ and p'_O is the effective overburden pressure at the point in question. If a point at $y = 5.5$ m is used as representative point of the entire soil layer before the 10 m of excavation, the effective overburden pressure becomes $p'_O = (11 - 5.5) \cdot (\gamma_{sat} - \gamma_w) + 10 \cdot \gamma_{unsat} = 212$ kPa. This leads to $\psi = 1.1$ implying $\alpha = R_{inter} = 0.492$.

A parametric analysis shows that the maximum heave of the excavation level is polynomially decreasing with increasing R_{inter} as seen in Fig. 7. The maximum heave is found at distances 150–200 mm from the pile shaft. The maximum heave is found to be approaching the heave of the soil excluding the pile. This indicates that the horizontal extent of the model is adequately.

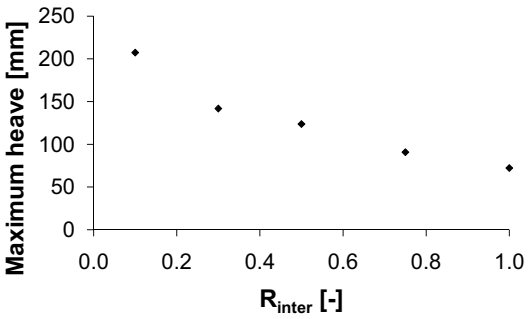

Figure 7: Maximum heave of the excavation level as a function of the strength reduction factor R_{inter}.

The analysed numerical models are listed in Tab. 4.

Table 4: Analysed models.

Model no.	Incl. pile	Pile load	Strength parameters
1	No	No	Undrained
2	No	No	Drained
3	Yes	No	Drained

Only the models excluding the pile make use of both the drained and the undrained strength parameters. The application of solely the drained strength parameters for the remaining model is the

result of numerical problems experienced by the authors when applying undrained strength parameters.

4 Validation of the Geometrical Model of Soil

To validate the geometrical model of a swelling soil by use of PLAXIS, an axisymmetric model solely consisting of soil is constructed. In addition, the influence of the applied material model is also analysed by plotting the results when applying both the Mohr-Coulomb material model and the Hardening Soil. When applying the MC material model, the reference value of Young's modulus of elasticity is chosen equal to E_{oed}.

Additionally, both drained and undrained strength parameters are applied for both material models. This is chosen because both the drained and undrained parameters give rise to problems when implemented in undrained material models. When applying undrained strength parameters, the parameters are interpreted as drained strength parameters because undrained behaviour is analysed by the effective stresses in PLAXIS. When using the effective strength parameters combined with the undrained soil behaviour, the mean effective stress p' for a Mohr-Coulomb material is constant up to failure. In nature, the development of p' is somewhat different, cf. Fig. 8. Hence, both drained and undrained strength parameters are investigated for modelling undrained behaviour.

The outer dimensions and material properties are similar to the model described in Sec. 3 with the only exception

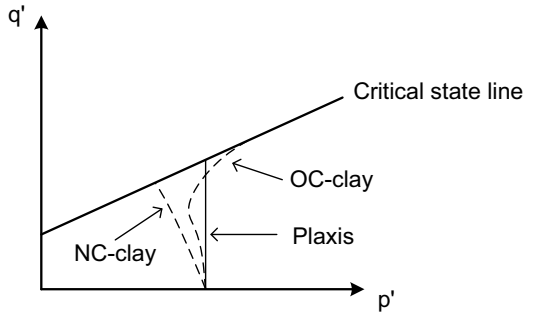

Figure 8: Effective stress paths for normally consolidated clay (NC-clay), overconsolidated clay (OC-clay) and for an undrained Mohr-Coulomb material with drained strength parameters defined in PLAXIS (Plaxis).

that the pile is not included. The model can be seen in Fig. 9.

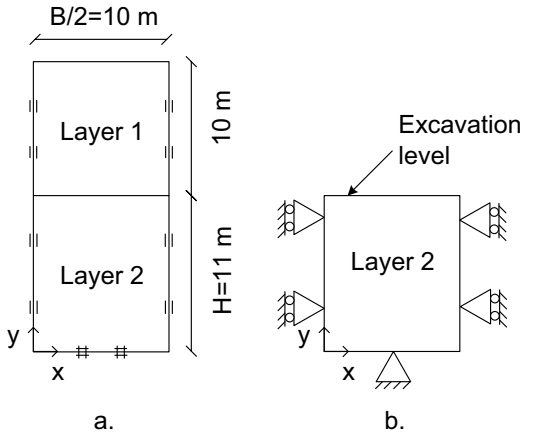

Figure 9: Model applied for numerical analysis of swelling soil in PLAXIS where the left vertical boundary is the axis of symmetry. a. Before excavation. b. After excavation.

The water level is located at the top of soil layer 2, i.e. at the excavation level. The mesh is constructed by 40 15-node elements with the global coarseness chosen as "Very Coarse" based on an analysis of convergence of the vertical displacement of the excavation level.

The boundary conditions of the soil mass are horizontal restraining $u_x = 0$ of the two vertical boundaries and horizontal and vertical restraining $u_x = u_y =$

0 of the lower boundary of the model, cf. Fig. 9. The vertical restraining of the lower boundary is chosen to ensure a reference line with zero vertical displacement. Hereby, the remaining vertical displacements of the soil body originate from displacements inside the model without influence of the subjacent soil layers. The horizontal restraining of both the lower boundary and the vertical boundaries are applied to ensure one-dimensional behaviour inside the soil body. This assumption agrees with the behaviour in nature where the surrounding soil of large horizontal extent functions as horizontal fixities.

The calculations consist of a plastic analysis of a staged construction simulating the excavation followed by a consolidation phase to model the swelling. During the calculations, the vertical boundaries and the horizontal lower boundary are modelled as *closed consolidation boundaries* to ensure no ground water flow through the boundaries.

4.1 Results of the Validation Analyses

A comparison between the effective stresses σ' immediately after the excavation determined by the submerged unit weight γ' and the depth and by PLAXIS revealed a satisfactory agreement between the two methods as seen in Fig. 10. The distributions of effective stresses through the soil are observed to be almost identical for both material models and for both drained and undrained strength parameters and are, thus, plotted combined as the "FEM" points in the figure. The maximum deviation is converged at a value of 2 %. The effective stress variation corresponds to the hatched red area in Fig. 1a. Skempton's

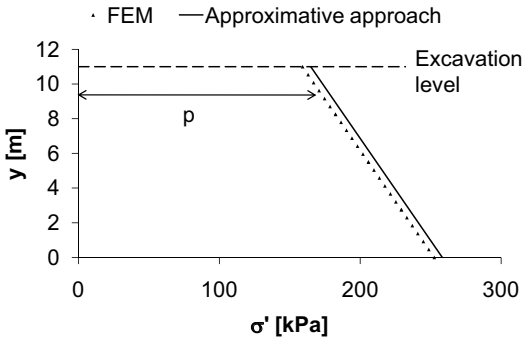

Figure 10: Effective stresses calculated by PLAXIS and the approximative approach of γ' and the depth through the axis of symmetry. $y = 0$ is the lower horizontal boundary of the model. $p = \gamma_{unsat} \cdot 10$ m is the unloading pressure.

coefficients of pore pressure are $A = 1/3$ and $B = 1$ for the determination of pore pressure u by the unit weight of water γ_w, the depth and the negative excess pore pressure Δu. The distribution of the pore pressures immediately after the excavation through the soil calculated by PLAXIS are plotted in Fig. 11.

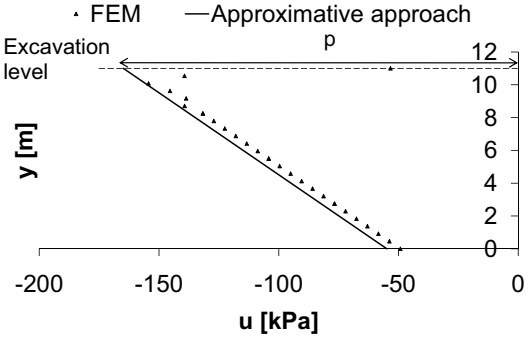

Figure 11: Pore pressures calculated by PLAXIS and the approximative approach of γ_w, Δu and the depth through the axis of symmetry. $y = 0$ is the lower horizontal boundary of the model. $p = \gamma_{unsat} \cdot 10$ m is the unloading pressure.

The distributions are observed to be almost identical for both material models and for both drained and undrained strength parameters. As seen in Fig. 11, there is a decrease in the absolute value of u near the excavation level which is not

included in the approximative approach. Besides the values near the excavation level, the maximum deviation is found to be 10 %.

In PLAXIS, water is slightly compressible leading to a decrease in Δu in compare to a non-compressible fluid. Being determined by Eqs. 5 and 6, this leads to a decrease in Skempton's coefficients of pore pressure and, hence, a deviation from the coefficients applied to the conventional theory (Krebs Ovesen et al., 2007; Brinkgreve et al., 2008b). This deviation may be the reason for the slightly higher deviation between the method of determining u than for the method of determining σ'. This is, however, assumed negligible. Thus, the pressure distribution through the soil is modelled satisfactorily.

$$A = \frac{\Delta u - \Delta\sigma_3}{\Delta\sigma_1 - \Delta\sigma_3} \quad (5)$$

$$B = \frac{\Delta u}{\Delta\sigma_3} \quad (6)$$

The heave of the excavation level determined by PLAXIS is compared to heave of preconsolidated clay defined in Eq. 7 as a frame of reference. Because $\Delta\sigma'$ is negative for the unloading situation, δ becomes positive.

$$\delta = -\frac{\Delta\sigma'}{E_{oed}} \cdot H \quad (7)$$

H is the thickness of the soil layer after excavation. The heave determined by Eq. 7 and by PLAXIS are plotted in Fig. 12.

As seen in Fig. 12, the choice of drained or undrained strength parameters does not influence the heave significantly. The material model, on the other hand, has great influence on the results. When applying the Mohr-Coulomb material models, the heave is close to the

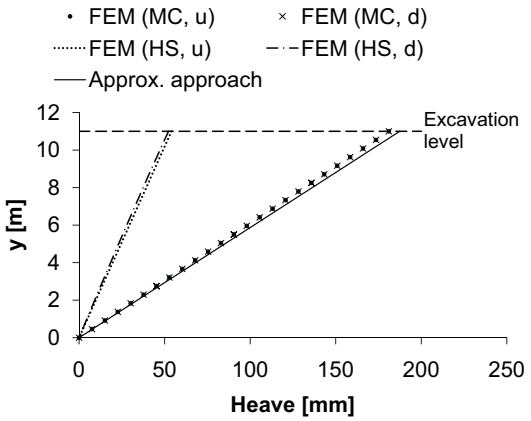

Figure 12: Heave calculated by PLAXIS (*FEM*) and the approximative approach of Eq. 7 through the axis of symmetry. $y = 0$ is the lower horizontal boundary of the model. u is for undrained and d for drained strength parameters.

approximative approach of Eq. 7. The deviation between the approximative approach and PLAXIS increases when applying the Hardening Soil material models. This could, however, be caused by the choice of Young's moduli of elasticity. Even though identical constrained moduli are applied for the two material models, the remaining moduli are chosen based on the relations $E_{50} = E_{oed}$ and $E_{ur} = 3 \cdot E_{oed}$ which influences the heave determined by the Hardening Soil material models. The heave determined by the Hardening Soil models are approximately 3.4 times smaller than by the Mohr-Coulomb models which indicates that the influencing parameter is the factor between E_{ur} and E_{oed}. This is substantiated by an analysis of the heave applying $E_{oed} = E_{ur} = 2 \cdot E_{50}$ where the heave of the HS-model is approximately 1.1 times smaller than of the MC-model.

The approximative approach of determining the heave by Eq. 7 leads to the largest results and is, thus, the most conservative of the applied methods based on the chosen Young's moduli of elasticity. This makes good sense because the approximative approach does not ac-

count for the increasing stiffness in unloading/reloading situations. Whether the Mohr-Coulomb or the Hardening Soil material model is closest to reality can only be evaluated by comparison with real observations of soil behaviour. This is, however, not covered by current analyses.

The maximum deviations between the results of PLAXIS and the approximative approaches are listed in Tab. 5. In addition to σ', u and the heave δ, the deviations of the negative excess pore pressures Δu calculated by PLAXIS compared to the theoretically determined values are also listed.

Table 5: Maximum deviation when applying the Hardening Soil and Mohr-Coulomb material models with undrained and drained strength parameters compared to the approximative approaches described above. δ is the heave.

Material model	σ'	Δu	u	δ
MC, undrained	2 %	3 %	10 %	6 %
MC, drained	2 %	3 %	10 %	6 %
HS, undrained	2 %	3 %	9 %	74 %
HS, drained	2 %	3 %	10 %	72 %

Overall, heave caused by an unloading to illustrate swelling is concluded to be modelled satisfactorily by the geometrical model.

5 Numerical Model of a Single Pile

A single pile is modelled in a cohesive soil exposed to unloading. Both model space, pile dimensions and material properties are based on the case study described in Sec. 3. The model can be seen in Fig. 13.

To illustrate the interaction between the soil and the pile, interfaces are applied

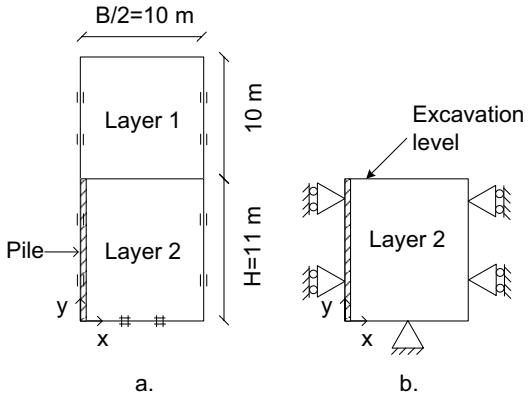

Figure 13: Model applied for numerical analyses of a single pile in swelling soil in PLAXIS where the left vertical boundary is the axis of symmetry. a. Before excavation. b. After excavation.

along the pile shaft. The interfaces are extended as seen in Fig. 14. This is implemented to avoid non-physical oscillations of stresses by enhancing the flexibility of the mesh and the number of nodes at the corners (Brinkgreve et al., 2008b).

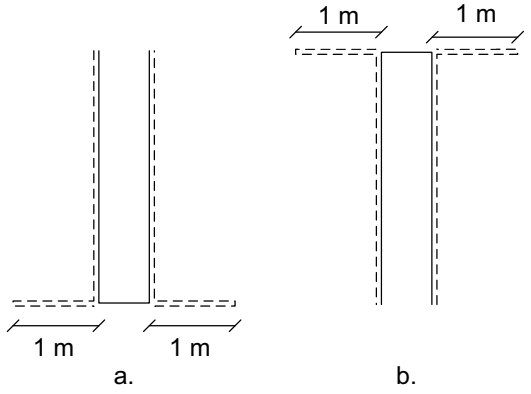

Figure 14: The applied interface between pile and soil. a. At $y = 0$. b. At $y = 11$ m.

The properties of the interface are connected to the surrounding soil materials by the strength reduction factor R_{inter} as described in Sec. 3. R_{inter} is determined by the cohesion of the soil materials and the desired cohesion of the interface of $c_i = 60$ kPa used for comparison to $R_{inter} = 0.267$.

The clay is modelled as an undrained Hardening Soil material with drained

strength parameters. The pile material is modelled as a non-porous linear elastic material. The input parameters are defined in Tab. 2. The stiffness of the concrete is chosen significantly higher than the stiffness of the clay to ensure a visible effect of the soil–pile interaction.

The mesh is constructed by 1345 15-node elements with the global coarseness chosen as "Very Fine" based on an analysis of convergence of the heave of the excavation level.

The calculations consist of a plastic analysis of a staged construction simulating the excavation, a plastic analysis of a staged construction illustrating the installation of the pile and a consolidation phase to illustrate the swelling process. During the calculations, the vertical boundaries and the horizontal lower boundary are modelled as *closed consolidation boundaries*.

5.1 Results of the Numerical Model

The results are determined on the basis of nodal points A through N and cross-sections O-O through R-R defined in Fig. 15. It should be noted that the heave in the cross-sections is determined on the basis of interpolation between heave in nearby nodal points. In addition, stresses in the cross-sections as well as at the points are determined on the basis of extrapolation from nearby stress points. The approximations are assumed adequate. (Brinkgreve et al., 2008b)

The maximum values of the heave and shear stresses at points A through N are listed in Tab. 6. On the basis of the heave of points A and G, the pile is seen to

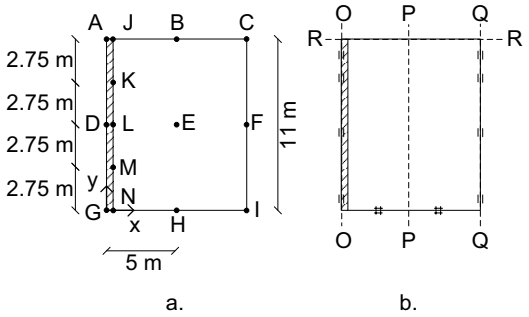

Figure 15: a. Definitions of points A through N. b. Definitions of cross-sections O-O through R-R.

be elongated 0.5 mm corresponding to 0.04 mm/m which seems realistic.

The heave through the cross-section O-O, i.e. through the pile, and through the cross-sections P-P and Q-Q, i.e. through the soil and at the right vertical boundary, can be seen in Fig. 16.

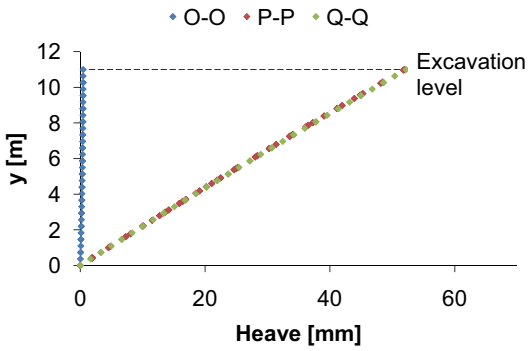

Figure 16: Vertical displacements through the cross-sections O-O through Q-Q. $y = 0$ m is the lower horizontal boundary of the model and $y = 11$ m is the level of the pile head, i.e. the excavation level.

As seen in the figure, the development of the heave is approximately identical for the cross-sections P-P and Q-Q indicating that the horizontal extent of the model is adequate. It also shows that neither the pile nor the mesh has any significant influence at these positions. This is substantiated by plotting the heave of the excavation level as seen in Fig. 17. From around $x = 1$ m, the heave is approximately constant. The deviation of the heave of the

Table 6: Maximum heave δ and shear stresses τ_i. Values separated by an oblique refer to displacements of pile and soil, respectively.

Point	A	B	C	D	E	F	G	H	I	J	K	L	M	N
x [m]	0	5	10	0	5	10	0	5	10	0.17	0.17	0.17	0.17	0.17
y [m]	11	11	11	5.5	5.5	5.5	0	0	0	11	8.25	5.5	2.75	0
δ [mm]	0.5	52	52	0.3	25	25	0	0	0	0.5/0.5	0.4/36	0.3/23	0.2/11	0/0.1
τ_i [kPa]	-	-	-	-	-	-	-	-	-	0.1	−20	−22	−24	−0.4

excavation level at 1 m$< x \leq$ 10 m from the heave of the excavation level for the model excluding the pile is less than 1 %. This implies a radius of influence of the pile of about 1 m corresponding to approximately 3 pile diameters.

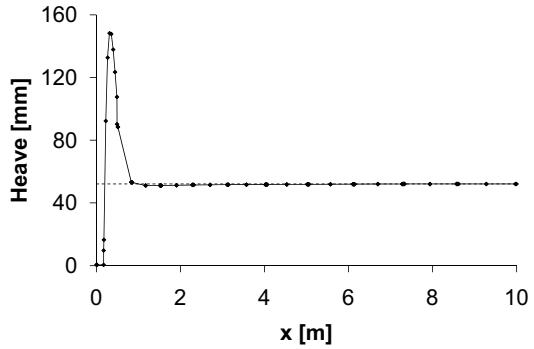

Figure 17: Heave through the cross-section Q-Q, i.e. at the excavation level. $x = 0$ m is the axis of symmetry and $x = 10$ m is the right vertical boundary of the model. The dashed line indicates the heave of the excavation level at the right vertical boundary.

As seen in Fig. 17, the soil close to the pile heaves significantly more than far from the pile. This is caused by the choice of the strength reduction factor $R_{inter} = 0.267$ which defines the strength of the interface as reduced strength parameters of the soil. This is substantiated by Fig. 18 where the heave of the excavation level is plotted as a function of R_{inter}. It can be seen in the figure that when R_{inter} approaches 1, i.e. the strength of the interface is equal to the strength of the soil, the heave close to the pile approaches the heave of the soil far from the pile.

Evidently, not only the soil at the interface but also the soil up to $3D$ from the centre line of the pile is affected by this "weakening". Thus, installation of unloaded piles with diameter D in swelling clays creates weak zones in a radius of $3D$ from the centre of the pile.

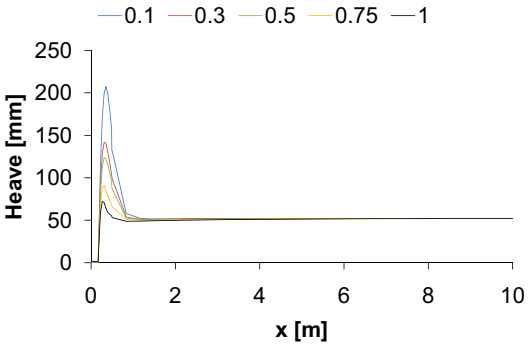

Figure 18: Heave of the excavation level as a function of R_{inter}.

Since heave is a result of changes in stresses, the effective stresses close to the soil–pile interface ($x = 0.18$ m), inside the weak soil ($x = 0.42$ m) and in the unaffected soil ($x = 2.0$ m) are plotted, cf. Figs. 19–21.

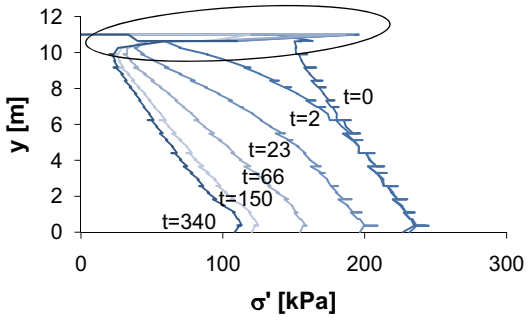

Figure 19: Effective stresses σ' through a vertical cross section at $x = 0.18$ m at different times. t is in years.

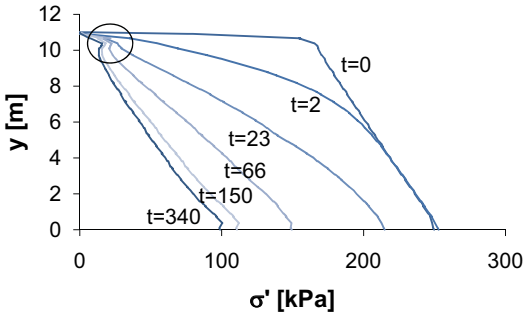

Figure 20: Effective stresses σ' through a vertical cross section at $x = 0.42$ m at different times. t is in years.

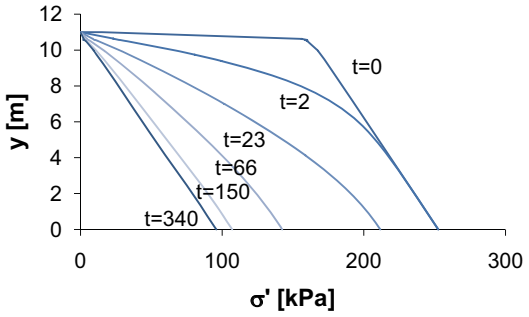

Figure 21: Effective stresses σ' through a vertical cross section at $x = 2.0$ m at different times. t is in years.

As seen in Fig. 19, significant increases in σ' are observed at $y = 10 - 11$ m. A slight increase in σ' can also be seen in Fig. 20 but clearly not as large as close to the soil–pile interface. As seen in Fig. 21, the effect of the pile cannot be observed in the development of σ' with time and depth. This indicates a connection between the local heave and the effective stresses at the upper 1 m of the soil in a radius of approximately $3D$ from the pile centre.

In Fig. 22, the heave at the points J through N at the soil–pile interface are plotted. When applying 15-node soil elements, the interface elements are defined by five pairs of nodes (Brinkgreve et al., 2008b). Hereby, the heave at the interface is determined both for the node connected to the pile and for the node connected to the soil leading to the two curves in Fig. 22. Since the interface elements have zero thickness, the coordinates of each node pair are identical.

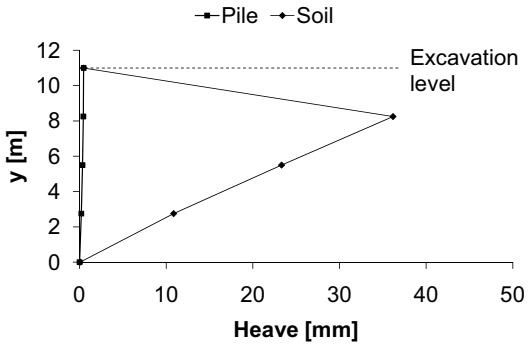

Figure 22: Heave at the points J through N at the interface.

As seen in the plot, the heave of the soil nodes at the interface are approximately equal to the heave of the pile nodes of the interface at the lower boundary of the model and at the pile head. At the remaining depths, the soil is exposed to up to 80 times the heave of the pile which implies shear stresses at the interface.

In Fig. 23, the shear stresses at the interface τ_i between the pile shaft and the soil are plotted. As seen in the figure, the interface is partly plastic indicated by the red dots. The Coulomb failure criterion for the interface is given in Eq. 8 for $\tan\varphi'_i = R_{inter} \cdot \tan\varphi' = \tan(4.4^\circ)$ and $c'_i = R_{inter} \cdot c' = 10.7$ kPa.

$$\begin{aligned} \tau_{max} &= \sigma'_N \cdot \tan\varphi'_i + c'_i \qquad (8) \\ \tau_{max} &= \sigma'_N \cdot \tan(4.4^\circ) + 10.7\ kPa \end{aligned}$$

σ'_N is the effective normal stress at the failure line at the interface. As seen in Fig. 23, the shear stresses are negative along the entire soil–pile interface. Since shear stresses are defined positive in the upward direction, cf. Brinkgreve et al. (2008b), the distribution indicates larger heave for the soil than for the pile. This was also observed by the heave shown in Fig. 22.

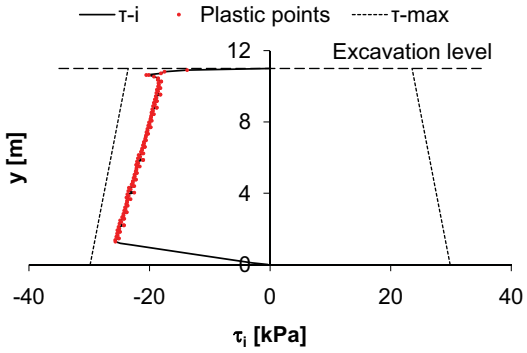

Figure 23: Shear stresses at the interface between pile shaft and soil. τ_{max} is the Coulomb failure criterion.

In Fig. 24, the heave at the points A and D are plotted as functions of time. As seen in Fig. 24, the heave at point A is larger than at point D. This is expected because point A is situated further from the line of zero displacement at $y = 0$ than point D and is, thus, exposed to additional upward displacements. Additionally, it can be seen in the figure that the maximum heave is not at the end of the swelling phase, i.e. 340 years, but after about 40 years. From 40–340 years the pile is no longer elongating but shrinking.

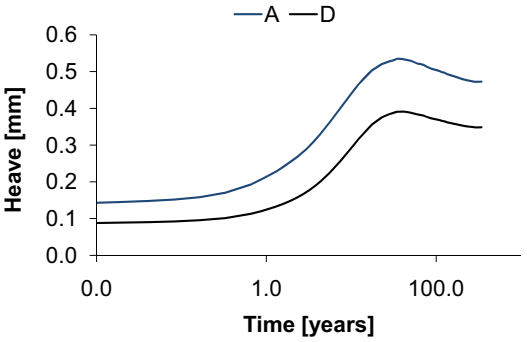

Figure 24: Heave at the points A and D as functions of time.

As seen in Fig. 25, the strength reduction factor R_{inter} does not influence this development of heave over time.

In Fig. 26, the percentage of the pile shaft where the soil–pile interface is plastic is plotted as a function of time. As seen in the figure, the percentage of plastic interface approaches an asymptotic value of 90 % corresponding to a plastic interface at 1.2 m $< y <$ 11 m. After 40 years, i.e. the time at which the heave in the pile starts to decrease, the interface is 74 % plastic corresponding to a plastic interface at 2.8 m $< y <$ 11 m. This indicates that the development of plastic interface implies the shrinkage of the pile because of the slip at the pile surface.

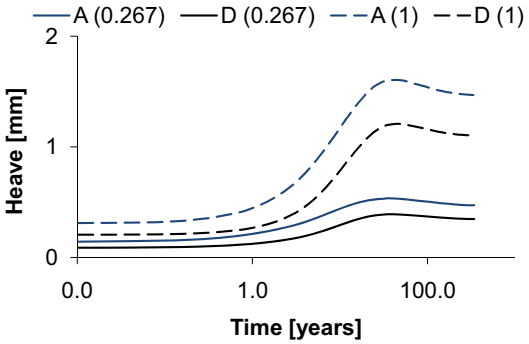

Figure 25: Heave at the points A and D as functions of time with $R_{inter} = 0.267$ and $R_{inter} = 1$.

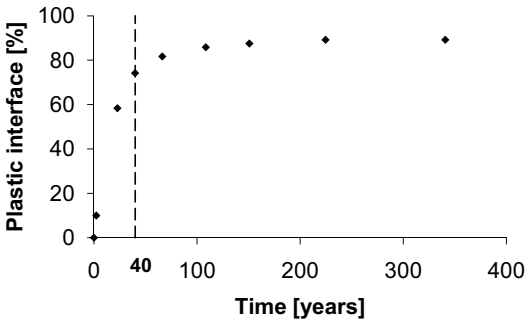

Figure 26: Percentage of the pile shaft which is plastic.

In Fig. 27, the heave at the points B, C, E and F are plotted as functions of time. It can be seen that the progress of the heave is identical for points in similar depths. Additionally, the heave at points B and C are larger than at points E and F as expected. The soil is fully swelled after 340 years.

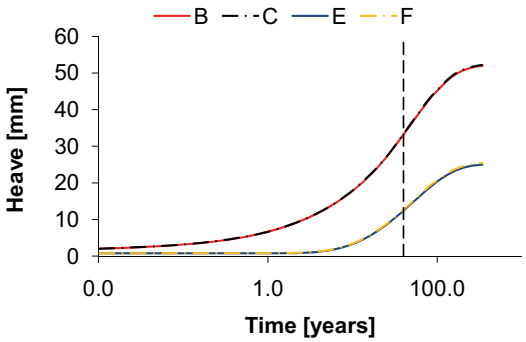

Figure 27: Heave at the points B, D, E and F as a function of time. The dashed line indicates 40 years, i.e. the time at which the heave in the pile starts to decrease.

The internal vertical stresses in the pile are determined in stress points through the pile from $y = 0$ to $y = 11$ m. The maximum value is found to $\sigma_{yy} = 2600$ kPa at the lowermost stress point after 50 years. It should be noted, though, that the maximum sum of internal vertical stresses through the pile is found to appear after approximately 35 years. This indicates a connection with the time at which the heave in the pile starts to decrease, cf. Fig. 24. The internal stresses through the pile after 50 years can be seen in Fig. 28.

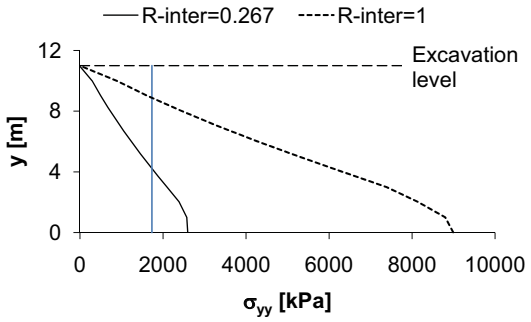

Figure 28: Internal vertical stresses through the pile after 50 years. The vertical blue line indicates the tensile strength of concrete with compressive strength of 30 MPa.

If, for example, the pile material is concrete with the compressive strength of $f_{ck} = 30$ MPa, the tensile strength can be approximated as $f_{ctk} = 1.7$ MPa by Eq. 9 (Jensen, 2007). Hence, tensile reinforcement is necessary to avoid failure of the pile.

$$f_{ctk} = \sqrt{0.1 \cdot f_{ck}} \tag{9}$$

In Fig. 28, the internal vertical stresses are also plotted for $R_{inter} = 1$. As seen in the figure, the stresses increase with increasing R_{inter} as expected.

6 Conclusions

For the investigated case study, the presence of the pile is observed to influence the heave in a radius of approximately 1 m, corresponding to 3 pile diameters D, from the axis of symmetry of the pile. The heave outside this radius is almost completely undisturbed by the pile with deviations from a model solely consisting of a swelling soil smaller than 1 %.

The heave inside the radius of influence is dependent on the strength reduction factor R_{inter}. The parametric analysis shows that the maximum heave of the excavation level is polynomially decreasing with increasing R_{inter}. However, for all investigated values of R_{inter}, the heave inside the radius of influence has shown to be larger than outside this radius. This indicates a weakening of the soil not only directly at the interface but up to $3D$ from the centre of the pile which should be further investigated. To minimise this effect, it is recommended to use piles with as rough surfaces as possible.

The choice of material model is seen to affect the heave significantly. Especially, the relation between the unloading–reloading modulus E_{ur} and the constrained modulus E_{oed} has great influence on the results and should be chosen carefully.

The swelling of the surrounding soil has shown to imply upward shear stresses at the soil–pile interface. This leads to tensile vertical stresses in the pile which in the current case exceed the tensile strength of concrete. Hence, it is necessary to take tensile reinforcement into account in design situations. The strength reduction factor R_{inter} influences significantly both the shear stresses at the interface and, hence, the internal vertical stresses in the pile. This factor should consequently be chosen with care.

During the swelling process modelled as a consolidation phase in PLAXIS, the pile has shown to be elongated to a maximum value after 35-40 years followed by some shrinkage up to the end of the swelling period of 340 years. It appears that the development of plastic interface implies the shrinkage of the pile because of the slip at the pile surface. This affects the internal stresses in the pile where the maximum values are observed after 35-50 years. Hence, when designing unloaded piles with a life expectancy of 100 years, the tensile stresses in the pile can be evaluated after the first 33–50 % of the design period.

Bibliography

Abbas, J. M., Z. H. Chika, and M. R. Taha (2008). Single pile simulation and analysis subjected to lateral load. *Electronic Journal of Geotechnical Engineering 13*(E), 1–15.

API (2000). *Recommended Practice for Planning, Designing and Constructing Fixed Offshore Platforms - Working Stress Design*. American Petroleum Institute.

Brinkgreve, R. B. J., W. Broere, and D. Waterman (2008a). *PLAXIS 2D Material Models Manual - Version 9.0*. PLAXIS bv.

Brinkgreve, R. B. J., W. Broere, and D. Waterman (2008b). *PLAXIS 2D Reference Manual - Version 9.0*. PLAXIS bv.

Harremoës, P., H. Moust Jacobsen, and N. Krebs Ovesen (1997). *Lærebog i GEOTEKNIK 1* (5th ed.). Århus, Denmark: Polyteknisk Forlag.

Jensen, B. C. (2007). *Betonkonstruktioner efter DS 411* (3rd ed.). Nyt Teknisk Forlag.

Krebs Ovesen, N., L. D. Fuglsang, and G. Bagge (2007). *Lærebog i Geoteknik* (1st ed.). Lyngby, Denmark: Polyteknisk Forlag.

Moust Jacobsen, H. and K. Gwizdala (1992). *Bearing capacity and settlements of piles*. Aalborg, Denmark: Centertrykkeriet, Aalborg University.

Okkels, N. and K. Bødker (2008). Beregning af hævninger under antagelse af retlinjet dræning. In *Nordisk Geoteknikermøde no. 15*, Sandefjord, Norway, pp. 383–389.

Poulos, H. G. and E. H. Davis (1980). *Pile foundation analysis and design* (1st ed.). John Wiley and sons.

Thøgersen, L. (2001). *Effects of Experimental Techniques and Osmotic Pressure on the Measured Behaviour of Tertiary Expansive Clay, Volume 1*. Ph. D. thesis, Soil Mechanics Laboratory, Aalborg University.

Recent publications in the DCE Technical Report Series

Kaufmann, K. L., Nielsen, B. N., & Augustesen, A. H. (2010). Strength and Deformation Properties of Tertiary Clay at Moesgaard Museum. *DCE Technical Report, 103*.

ISSN 1901-726X
DCE Technical Report No. 104